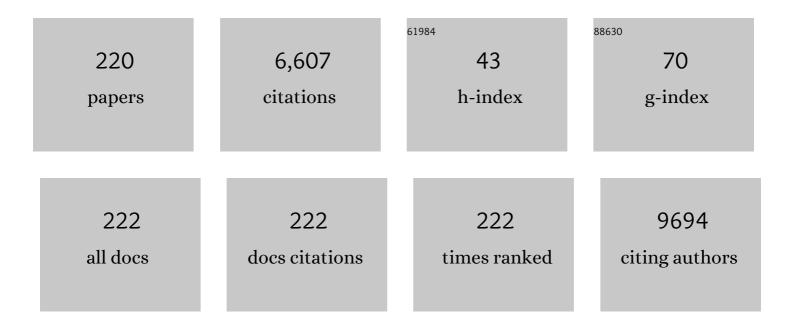
Zheng Jun Zhang

List of Publications by Year in descending order

Source: https://exaly.com/author-pdf/1786033/publications.pdf Version: 2024-02-01



#	Article	IF	CITATIONS
1	Research progress of SERS on uranyl ions and uranyl compounds: a review. Journal of Materials Chemistry C, 2022, 10, 4006-4018.	5.5	8
2	Tailoring TiO ₂ /Al ₂ O ₃ heterolayers as optical filters for the visible region. Nanoscale Advances, 2022, 4, 1608-1616.	4.6	2
3	Platinum doped bismuth vanadate (Pt/BiVO4) for enhanced photocatalytic pollutant degradation using visible light irradiation. Journal of Materials Science: Materials in Electronics, 2022, 33, 15116-15131.	2.2	5
4	Coupling between Surface Plasmon Modes of Single-Layer Complex Silver Nanohole Arrays and Enhancing Index Sensing. ACS Applied Nano Materials, 2022, 5, 9761-9770.	5.0	6
5	Robust quantitative SERS analysis with Relative Raman scattering intensities. Talanta, 2021, 221, 121465.	5.5	22
6	Preparation of a superhydrophobic TiN/PTFE composite film toward self-cleaning and corrosion protection applications. Journal of Materials Science, 2021, 56, 1413-1425.	3.7	27
7	TiO2 nanorod arrays decorated with Au nanoparticles as sensitive and recyclable SERS substrates. Journal of Alloys and Compounds, 2021, 861, 157999.	5.5	31
8	The effect of nanorod position on the plasmonic properties of the complex nanorod in nanohole arrays. Journal Physics D: Applied Physics, 2021, 54, 155201.	2.8	6
9	Construction of 1T-MoS ₂ quantum dots-interspersed (Bi _{1â^x} Fe _x)VO ₄ heterostructures for electron transport and photocatalytic properties. RSC Advances, 2021, 11, 13105-13118.	3.6	20
10	Nanometer-Thick Al ₂ O ₃ Layers on Ag–Al Nanostructures as Conductive Electrodes. ACS Applied Nano Materials, 2021, 4, 1270-1281.	5.0	1
11	Bismuth vanadate/MXene (BiVO4/Ti3C2) heterojunction composite: enhanced interfacial control charge transfer for highly efficient visible light photocatalytic activity. Environmental Science and Pollution Research, 2021, 28, 35911-35923.	5.3	23
12	Photocatalytic performance of ferric vanadate (FeVO4) nanoparticles synthesized by hydrothermal method. Materials Science in Semiconductor Processing, 2021, 129, 105785.	4.0	28
13	Performance of Transparent Metallic Thin Films. Journal of Physical Chemistry C, 2021, 125, 16334-16342.	3.1	2
14	Design and fabrication of nanorod in nanohole arrays with highly tunable enhanced optical transmission. , 2021, , .		0
15	Highly Conductive Nanograting–Nanohole Structures with Tunable and Dual-Band Spectral Transparency. ACS Applied Electronic Materials, 2021, 3, 3489-3500.	4.3	4
16	Non-invasive disease diagnosis using surface-enhanced Raman spectroscopy of urine and saliva. Applied Spectroscopy Reviews, 2020, 55, 197-219.	6.7	31
17	Ultrasensitive Fieldâ€Effect Biosensors Enabled by the Unique Electronic Properties of Graphene. Small, 2020, 16, e1902820.	10.0	75
18	Study of the interfacial charge transfer in bismuth vanadate/reduce graphene oxide (BiVO4/rGO) composite and evaluation of its photocatalytic activity. Research on Chemical Intermediates, 2020, 46, 1201-1215.	2.7	34

#	Article	IF	CITATIONS
19	Facile synthesis of Zn3(VO4)2/FeVO4 heterojunction and study on its photocatalytic and electrochemical properties. Applied Nanoscience (Switzerland), 2020, 10, 421-433.	3.1	20
20	The IR plasmonic properties of sub-wavelength ITO rod arrays predicted by anisotropic effective medium theory. Nanotechnology, 2020, 31, 075203.	2.6	0
21	Synthesis of novel visible light assisted Pt doped zinc vanadate (Pt/Zn4V2O9) for enhanced photocatalytic properties. Chemical Physics, 2020, 539, 110980.	1.9	13
22	Detection of corrosion inhibitor adsorption via a surface-enhanced Raman spectroscopy (SERS) silver nanorods tape sensor. Sensors and Actuators B: Chemical, 2020, 321, 128617.	7.8	36
23	Large-Area Fabrication of Complex Nanohole Arrays with Highly Tunable Plasmonic Properties. ACS Applied Materials & Interfaces, 2020, 12, 37435-37443.	8.0	10
24	Design of Armrest Ag Nanorod Arrays with High SERS Performance for Sensitive Biomolecule Detection. Journal of Physical Chemistry C, 2020, 124, 21054-21062.	3.1	14
25	Facile synthesis of Se/BiVO4 heterojunction composite and evaluation of synergetic reaction mechanism for efficient photocatalytic staining of organic dye pollutants in wastewater under visible light. Journal of Materials Science: Materials in Electronics, 2020, 31, 19599-19612.	2.2	13
26	Efficient Hydrogen Evolution Reaction on Ni3S2 Nanorods with a P/N Bipolar Electrode Prepared by Dealloying Sulfurization of NiW Amorphous Alloys. ACS Applied Energy Materials, 2020, 3, 5745-5755.	5.1	7
27	Formation and Properties of Amorphous Multi-Component (CrFeMoNbZr)Ox Thin Films. Metals, 2020, 10, 599.	2.3	3
28	Morphological effects on the photocatalytic performance of FeVO4 nanocomposite. Nano Structures Nano Objects, 2020, 22, 100431.	3.5	31
29	Coupling between plasmonic nanohole array and nanorod array: the emerging of a new extraordinary optical transmission mode and epsilon-near-zero property. Journal Physics D: Applied Physics, 2020, 53, 275202.	2.8	16
30	A high-strength Co–Fe–Ta–B metallic-glass phase enabled tensile plasticity in Co–Fe–Ta–B–O oxio glass matrix nanocomposites. Applied Physics Letters, 2020, 116, .	de _{3.3}	7
31	Quantum sieving of H ₂ /D ₂ in MOFs: a study on the correlation between the separation performance, pore size and temperature. Journal of Materials Chemistry A, 2020, 8, 6319-6327.	10.3	13
32	Preparation and characterization of Vanadium pentoxide (V2O5) for photocatalytic degradation of monoazo and diazo dyes. Surfaces and Interfaces, 2020, 19, 100502.	3.0	60
33	10.1063/1.5143598.2. , 2020, , .		0
34	Flexible and adhesive tape decorated with silver nanorods for in-situ analysis of pesticides residues and colorants. Mikrochimica Acta, 2019, 186, 603.	5.0	26
35	Fishnet-like Ni–Fe–N co-modified graphene aerogel catalyst for highly efficient oxygen reduction reaction in an alkaline medium. Journal of Applied Electrochemistry, 2019, 49, 1211-1226.	2.9	3
36	Surface-enhanced ZnS:Ag quantum dots scintillator. AIP Advances, 2019, 9, 105211.	1.3	1

#	Article	IF	CITATIONS
37	Large lattice mismatch induced perpendicular magnetic anisotropy and perpendicular exchange bias in CoPt/FeMn bilayer films. Science China Technological Sciences, 2019, 62, 2009-2013.	4.0	6
38	Amorphous magnetic semiconductors with Curie temperatures above room temperature. Journal of Semiconductors, 2019, 40, 081510.	3.7	9
39	Direct observation of fast surface dynamics in sub-10-nm nanoglass particles. Applied Physics Letters, 2019, 114, 043103.	3.3	12
40	Plasmon-mediated photothermal and superhydrophobic TiN-PTFE film for anti-icing/deicing applications. Composites Science and Technology, 2019, 181, 107696.	7.8	105
41	Simultaneous Thermal Stability and Ultrahigh Sensitivity of Heterojunction SERS Substrates. Nanomaterials, 2019, 9, 830.	4.1	14
42	The evolution of He+ irradiation-induced point defects and helium retention in nuclear graphite. Journal of Nuclear Science and Technology, 2019, 56, 744-751.	1.3	2
43	Fast Surface Charge Transfer with Reduced Band Gap Energy of FeVO4/Graphene Nanocomposite and Study of Its Electrochemical Property and Enhanced Photocatalytic Activity. Arabian Journal for Science and Engineering, 2019, 44, 6659-6667.	3.0	21
44	Ag Nanorods-Based Surface-Enhanced Raman Scattering: Synthesis, Quantitative Analysis Strategies, and Applications. Frontiers in Chemistry, 2019, 7, 376.	3.6	12
45	Microstructure evolution and Young's modulus of He-implanted nanocrystalline tungsten film. Journal of Nuclear Materials, 2019, 518, 226-233.	2.7	11
46	Hydrothermal fabrication of monoclinic bismuth vanadate (m-BiVO4) nanoparticles for photocatalytic degradation of toxic organic dyes. Materials Science and Engineering B: Solid-State Materials for Advanced Technology, 2019, 242, 83-89.	3.5	61
47	Effects of Ti transition layers and thermal annealing on the adhesive property of Ag nanorods-based SERS sensors. Applied Surface Science, 2019, 476, 363-368.	6.1	9
48	Slanted Ag-Al alloy nanorods arrays for highly active and stable surface-enhanced Raman scattering substrates. Nanotechnology, 2019, 30, 235703.	2.6	4
49	TiN Nanorods as Effective Substrate for Surface-Enhanced Raman Scattering. Journal of Physical Chemistry C, 2019, 123, 29353-29359.	3.1	21
50	Strong long-range perpendicular exchange bias across a spacer layer. AIP Advances, 2019, 9, 125046.	1.3	2
51	Label-free surface-enhanced Raman spectroscopy of serum based on multivariate statistical analysis for the diagnosis and staging of lung adenocarcinoma. Vibrational Spectroscopy, 2019, 100, 177-184.	2.2	25
52	Standing wave type localized surface plasmon resonance of multifold Ag nanorods. Nanotechnology, 2019, 30, 055703.	2.6	5
53	AMORPHIZATION OF CERIUM MONONITRIDE DURING OXIDIZATION CHARACTERIZED BY OPTICAL MICROSCOPY, SCANNING ELECTRON MICROSCOPY, X-RAY DIFFRACTION AND X-RAY PHOTOELECTRON SPECTROSCOPY. Surface Review and Letters, 2019, 26, 1850180.	1.1	0
54	Facile synthesis of Zinc vanadate Zn3(VO4)2 for highly efficient visible light assisted photocatalytic activity. Journal of Alloys and Compounds, 2019, 775, 281-289.	5.5	52

#	Article	IF	CITATIONS
55	Surface-Enhanced Raman Scattering Detection of Pesticide Residues Using Transparent Adhesive Tapes and Coated Silver Nanorods. ACS Applied Materials & Interfaces, 2018, 10, 9129-9135.	8.0	130
56	HfO2-wrapped slanted Ag nanorods array as a reusable and sensitive SERS substrate for trace analysis of uranyl compounds. Sensors and Actuators B: Chemical, 2018, 265, 539-546.	7.8	16
57	Bilayer SiO ₂ Nanorod Arrays as Omnidirectional and Thermally Stable Antireflective Coating. Advanced Engineering Materials, 2018, 20, 1700942.	3.5	14
58	Direct observation of heavy quasiparticles in the Kondo-lattice compound <mml:math xmlns:mml="http://www.w3.org/1998/Math/MathML"><mml:mrow><mml:mi>Cel</mml:mi><mml:msub><mml:mimathvariant="normal">n<mml:mn>3</mml:mn></mml:mimathvariant="normal"></mml:msub></mml:mrow></mml:math> . Physical Review B, 2018, 97, .	3.2	9
59	Emergence of Kondo lattice behavior in a van der Waals itinerant ferromagnet, Fe ₃ GeTe ₂ . Science Advances, 2018, 4, eaao6791.	10.3	157
60	Efficient photocatalysis with graphene oxide/Ag/Ag ₂ S–TiO ₂ nanocomposites under visible light irradiation. RSC Advances, 2018, 8, 5784-5791.	3.6	33
61	Detailed correlations between SERS enhancement and plasmon resonances in subwavelength closely spaced Au nanorod arrays. Nanoscale, 2018, 10, 4267-4275.	5.6	40
62	Mechanical properties and structure evolution of single-crystalline silicon irradiated by 1†MeV Au+ and Cu+ ions. Nuclear Instruments & Methods in Physics Research B, 2018, 423, 75-81.	1.4	1
63	Mechanically robust antireflective coatings. Nano Research, 2018, 11, 1699-1713.	10.4	22
64	Anisotropic ferromagnetism in Fe x Sn1â^'x O2 nanostructure arrays. Journal of Materials Science, 2018, 53, 3280-3288.	3.7	2
65	Hydrogen permeation properties of CrxCy@Cr2O3/Al2O3 composite coating derived from selective oxidation of a Cr C alloy and atomic layer deposition. International Journal of Hydrogen Energy, 2018, 43, 21133-21141.	7.1	20
66	Fabrication and simulation of V-shaped Ag nanorods as high-performance SERS substrates. Physical Chemistry Chemical Physics, 2018, 20, 25623-25628.	2.8	12
67	Highly stable and active SERS substrates with Ag–Ti alloy nanorods. Nanoscale, 2018, 10, 19863-19870.	5.6	23
68	Visible Light Driven Photoanodes for Water Oxidation Based on Novel r-GO/β-Cu2V2O7/TiO2 Nanorods Composites. Nanomaterials, 2018, 8, 544.	4.1	23
69	Phase control and Young's modulus of tungsten thin film prepared by dual ion beam sputtering deposition. AIP Advances, 2018, 8, .	1.3	20
70	Visible light assisted photocatalytic degradation of crystal violet dye and electrochemical detection of ascorbic acid using a BiVO ₄ /FeVO ₄ heterojunction composite. RSC Advances, 2018, 8, 23489-23498.	3.6	86
71	Unexpected large nanoparticle size of single dimer hotspot systems for broadband SERS enhancement. Optics Letters, 2018, 43, 2332.	3.3	30
72	Omnidirectional SiO2 AR Coatings. Coatings, 2018, 8, 210.	2.6	5

#	Article	IF	CITATIONS
73	The Effect of Annealing Treatment and Atom Layer Deposition to Au/Pt Nanoparticles-Decorated TiO2 Nanorods as Photocatalysts. Molecules, 2018, 23, 525.	3.8	19
74	Zigzag Localized Surface Plasmon Resonance Wavelength Shift of Asymmetric V-Shape Ag Nanorods. Journal of Physical Chemistry C, 2018, 122, 17400-17405.	3.1	3
75	Quantification of trace chemicals in unknown complex systems by SERS. Talanta, 2018, 186, 452-458.	5.5	15
76	HfO ₂ Nanorod Array as Highâ€Performance and Highâ€Temperature Antireflective Coating. Advanced Materials Interfaces, 2017, 4, 1600892.	3.7	16
77	Enhanced photocatalytic properties of CdS nanoparticles decorated α-Fe2O3 nanopillar arrays under visible light. Journal of Colloid and Interface Science, 2017, 494, 107-113.	9.4	24
78	Nanoparticle-on-mirror cavity modes for huge and/or tunable plasmonic field enhancement. Nanotechnology, 2017, 28, 105203.	2.6	40
79	SERS detection and characterization of uranyl ion sorption on Âsilver nanorods wrapped with Al2O3 layers. Mikrochimica Acta, 2017, 184, 2775-2782.	5.0	25
80	Novel [111] oriented γ-Mo2N thin films deposited by magnetron sputtering as an anode for aqueous micro-supercapacitors. Electrochimica Acta, 2017, 245, 237-248.	5.2	48
81	Analytical plasmon dispersion in subwavelength closely spaced Au nanorod arrays from planar metal–insulator–metal waveguides. Journal of Materials Chemistry C, 2017, 5, 6079-6085.	5.5	15
82	Antireflective Coatings: HfO ₂ Nanorod Array as Highâ€Performance and Highâ€Temperature Antireflective Coating (Adv. Mater. Interfaces 6/2017). Advanced Materials Interfaces, 2017, 4, .	3.7	0
83	Morphological influence of TiO 2 nanostructures (nanozigzag, nanohelics and nanorod) on photocatalytic degradation of organic dyes. Applied Surface Science, 2017, 400, 184-193.	6.1	95
84	Al ₂ O ₃ Encapsulated Teflon Nanostructures with High Thermal Stability and Efficient Antireflective Performance. ACS Applied Materials & Interfaces, 2017, 9, 36327-36337.	8.0	23
85	Semi-quantitative analysis of multiple chemical mixtures in solution at trace level by surface-enhanced Raman Scattering. Scientific Reports, 2017, 7, 6186.	3.3	19
86	Design of Ag nanorods for sensitivity and thermal stability of surface-enhanced Raman scattering. Nanotechnology, 2017, 28, 405602.	2.6	14
87	Dependence of the Thermal Conductivity of <mml:math xmlns:mml="http://www.w3.org/1998/Math/MathML" display="inline"><mml:mrow><mml:msub><mml:mrow><mml:mi>BiFeO</mml:mi></mml:mrow><mml:mrow>< Thin Films on Polarization and Structure. Physical Review Applied. 2017. 8</mml:mrow></mml:msub></mml:mrow></mml:math 	៣ភ <mark>ាំ!8</mark> ៣>3	<mark 31 <
88	Annealing effect on the photoelectrochemical and photocatalytic performance of TiO ₂ nanorod arrays. RSC Advances, 2017, 7, 51382-51390.	3.6	11
89	Ag Nanorods-Oxide Hybrid Array Substrates: Synthesis, Characterization, and Applications in Surface-Enhanced Raman Scattering. Sensors, 2017, 17, 1895.	3.8	8
90	Pyridinicâ€Nitrogenâ€Dominated Graphene Aerogels with Fe–N–C Coordination for Highly Efficient Oxygen Reduction Reaction. Advanced Functional Materials, 2016, 26, 5708-5717.	14.9	360

#	Article	IF	CITATIONS
91	Hybridized plasmon modes and near-field enhancement of metallic nanoparticle-dimer on a mirror. Scientific Reports, 2016, 6, 30011.	3.3	80
92	Three-dimensional bulk electronic structure of the Kondo lattice CeIn3 revealed by photoemission. Scientific Reports, 2016, 6, 33613.	3.3	8
93	Pinhole Effect on the Melting Behavior of Ag@Al2O3 SERS Substrates. Nanoscale Research Letters, 2016, 11, 170.	5.7	10
94	High-Performance Real-Time SERS Detection with Recyclable Ag Nanorods@HfO ₂ Substrates. ACS Applied Materials & Interfaces, 2016, 8, 27162-27168.	8.0	68
95	Synthesis of nitrogen-doped reduced graphene oxide as metal-free electrocatalyst for oxygen reduction reactions. International Journal of Nanomanufacturing, 2016, 12, 252.	0.3	0
96	Preparation of TiO _{2 nanorod arrays decorated with CdS nanoparticles exhibiting enhanced photoelectrochemical and photocatalytic properties in visible light. International Journal of Nanomanufacturing, 2016, 12, 237.}	0.3	0
97	Quantitative Analysis of Single and Mix Food Antiseptics Basing on SERS Spectra with PLSR Method. Nanoscale Research Letters, 2016, 11, 296.	5.7	18
98	Tunable Lattice Coupling of Multipole Plasmon Modes and Near-Field Enhancement in Closely Spaced Gold Nanorod Arrays. Scientific Reports, 2016, 6, 23159.	3.3	34
99	Glancing angle deposition of Fe triangular nanoprisms consisting of vertically-layered nanoplates. Journal of Crystal Growth, 2016, 451, 113-119.	1.5	2
100	Surface Plasmon Enhanced Photocatalysis of Au/Pt-decorated TiO2 Nanopillar Arrays. Scientific Reports, 2016, 6, 26670.	3.3	119
101	Role of Ag2S coupling on enhancing the visible-light-induced catalytic property of TiO2 nanorod arrays. Scientific Reports, 2016, 6, 19754.	3.3	20
102	Universal Near-Field Interference Patterns of Fano Resonances in Two-Dimensional Plasmonic Crystals. Plasmonics, 2016, 11, 1377-1383.	3.4	30
103	α-Fe ₂ O ₃ nanopillar arrays fabricated by electron beam evaporation for the photoassisted degradation of dyes with H ₂ O ₂ . RSC Advances, 2016, 6, 534-540.	3.6	7
104	Gradual plasmon evolution and huge infrared near-field enhancement of metallic bridged nanoparticle dimers. Physical Chemistry Chemical Physics, 2016, 18, 2319-2323.	2.8	19
105	Pinhole-Containing, Subnanometer-Thick Al ₂ O ₃ Shell-Coated Ag Nanorods as Practical Substrates for Quantitative Surface-Enhanced Raman Scattering. Journal of Physical Chemistry C, 2016, 120, 606-615.	3.1	39
106	Compositional Analysis of Ternary and Binary Chemical Mixtures by Surface-Enhanced Raman Scattering at Trace Levels. Nanoscale Research Letters, 2015, 10, 437.	5.7	14
107	Ag Nanorods Coated with Ultrathin TiO2 Shells as Stable and Recyclable SERS Substrates. Scientific Reports, 2015, 5, 15442.	3.3	72
108	Silver Nanorods Wrapped with Ultrathin Al2O3 Layers Exhibiting Excellent SERS Sensitivity and Outstanding SERS Stability. Scientific Reports, 2015, 5, 12890.	3.3	89

#	Article	IF	CITATIONS
109	Near-field mapping of three-dimensional surface charge poles for hybridized plasmon modes. AIP Advances, 2015, 5, .	1.3	20
110	Sensitivity and Reusability of SiO2 NRs@ Au NPs SERS Substrate in Trace Monochlorobiphenyl Detection. Nanoscale Research Letters, 2015, 10, 444.	5.7	15
111	X-ray irradiation-induced reversible wettability modification of titanium NRAs. RSC Advances, 2015, 5, 4524-4528.	3.6	2
112	Wettability manipulation of magnetic transition metal nanorod arrays by X-ray irradiation. Frontiers of Materials Science, 2015, 9, 311-315.	2.2	1
113	Tunable SERS-Tags-Hidden Gold Nanorattles for Theranosis of Cancer Cells with Single Laser Beam. Scientific Reports, 2015, 4, 6709.	3.3	21
114	Atomic oxygen treatment effects on magnetron sputtered Zr–Ti binary films. Applied Surface Science, 2015, 324, 669-676.	6.1	6
115	High-magnetic field annealing effect on room-temperature ferromagnetism enhancement of un-doped HfO2 thin films. Applied Physics A: Materials Science and Processing, 2015, 119, 917-921.	2.3	1
116	Reduced graphene oxide/carbon nanotube hybrid film as high performance negative electrode for supercapacitor. Electrochimica Acta, 2015, 169, 342-350.	5.2	139
117	200 keV Xe+ ions irradiation effects on Zr–Ti binary films. Nuclear Instruments & Methods in Physics Research B, 2015, 350, 26-31.	1.4	3
118	Defects-Driven Ferromagnetism in Undoped Dilute Magnetic Oxides: A Review. Journal of Materials Science and Technology, 2015, 31, 969-978.	10.7	49
119	Nanogap effects on near- and far-field plasmonic behaviors of metallic nanoparticle dimers. Physical Chemistry Chemical Physics, 2015, 17, 29293-29298.	2.8	67
120	Phase-dependent and defect-driven d ⁰ ferromagnetism in undoped ZrO ₂ thin films. RSC Advances, 2015, 5, 3636-3641.	3.6	32
121	Effect of Xe ion irradiation on photocatalytic performance of oblique TiO2 nanowire arrays. Applied Surface Science, 2015, 327, 478-482.	6.1	11
122	Well-aligned NiSi/Si heterostructured nanowire arrays as field emitters. Journal of Vacuum Science and Technology B:Nanotechnology and Microelectronics, 2015, 33, .	1.2	15
123	Enhanced photoelectrochemical and photocatalytic performance of TiO2 nanorod arrays/CdS quantum dots by coating TiO2 through atomic layer deposition. Nano Energy, 2015, 11, 400-408.	16.0	104
124	Facile decolorization of methylene blue with flower-like manganese wads. Water Science and Technology, 2014, 69, 1094-1100.	2.5	3
125	CO ₂ corrosion of IG-110 nuclear graphite studied by gas chromatography. Journal of Nuclear Science and Technology, 2014, 51, 487-492.	1.3	13
126	Enhanced photoelectrochemical properties of TiO ₂ nanorod arrays decorated with CdS nanoparticles. Science and Technology of Advanced Materials, 2014, 15, 055006.	6.1	34

#	Article	IF	CITATIONS
127	Mechanical property improvement by texture control of magnetron co-sputtered Zr-Ti films. Journal of Applied Physics, 2014, 115, .	2.5	11
128	Synthesis of flower-like manganese wad and its decolorization performance for azo dye Congo red. Chemical Research in Chinese Universities, 2014, 30, 306-309.	2.6	1
129	Tunable field emission properties of well-aligned silicon nanowires with controlled aspect ratio and proximity. RSC Advances, 2014, 4, 31729-31734.	3.6	13
130	Fabrication of TiN nanostructure as a hydrogen peroxide sensor by oblique angle deposition. Nanoscale Research Letters, 2014, 9, 105.	5.7	16
131	Enhanced light absorption of amorphous silicon thin film by substrate control and ion irradiation. Nanoscale Research Letters, 2014, 9, 173.	5.7	14
132	Enhancement of the photocatalytic property of TiO2 columnar nanostructured films by changing deposition angle. Materials Research Bulletin, 2014, 50, 68-72.	5.2	15
133	The Ti@MoOx nanorod array as a three dimensional film electrode for micro-supercapacitors. Electrochemistry Communications, 2014, 44, 23-26.	4.7	15
134	Fabrication of MoO <i>_x</i> Film as a Conductive Anode Material for Micro-Supercapacitors by Electrodeposition and Annealing. Journal of the Electrochemical Society, 2014, 161, A1051-A1057.	2.9	12
135	Molybdenum oxide film with stable pseudocapacitive property for aqueous micro-scale electrochemical capacitor. Electrochimica Acta, 2014, 134, 84-91.	5.2	21
136	The fabrication of large-scale sub-10-nm core-shell silicon nanowire arrays. Nanoscale Research Letters, 2013, 8, 405.	5.7	25
137	Tuning the optical bandgap of TiO2-TiN composite films as photocatalyst in the visible light. AIP Advances, 2013, 3, .	1.3	29
138	Indirect to direct band gap transition in ultra-thin silicon films. Physical Chemistry Chemical Physics, 2013, 15, 6063.	2.8	37
139	Origin of the defects-induced ferromagnetism in un-doped ZnO single crystals. Applied Physics Letters, 2013, 102, .	3.3	67
140	The Regulation of Surface-Enhanced Raman Scattering Sensitivity of Silver Nanorods by Silicon Sections. Journal of Nanomaterials, 2013, 2013, 1-5.	2.7	3
141	Visible Light Photoelectrochemical Properties of N-Doped TiO2Nanorod Arrays from TiN. Journal of Nanomaterials, 2013, 2013, 1-8.	2.7	9
142	MoO _{<i>x</i>} thin films deposited by magnetron sputtering as an anode for aqueous micro-supercapacitors. Science and Technology of Advanced Materials, 2013, 14, 065005.	6.1	26
143	Room-temperature ferromagnetism in un-doped ZrO ₂ thin films. Journal Physics D: Applied Physics, 2013, 46, 445004.	2.8	50
144	Microstructure and Properties of Pure Zirconium After Irradiation by Charged Particles. Thirty Years of Astronomical Discovery With UKIRT, 2013, , 417-426.	0.3	1

#	Article	IF	CITATIONS
145	The Nanofabrication and Application of Substrates for Surface-Enhanced Raman Scattering. International Journal of Spectroscopy, 2012, 2012, 1-7.	1.6	8
146	Photocatalytic Properties of Columnar Nanostructured <mml:math xmlns:mml="http://www.w3.org/1998/Math/MathML"><mml:mrow><mml:msub><mml:mrow><mml:mrow><mml:mtext>TiC mathvariant="bold">2</mml:mtext></mml:mrow></mml:mrow></mml:msub></mml:mrow>Films Fabricated by Sputtering Ti and Subsequent Annealing. Advances in Materials Science and Engineering, 2012, 2012, 1-5.</mml:math) <td>text_g </td>	text _g
147	The Influence of Pores on Irradiation Property of Selected Nuclear Graphites. Advances in Materials Science and Engineering, 2012, 2012, 1-6.	1.8	5
148	Effects of Porosity and Temperature on Oxidation Behavior in Air of Selected Nuclear Graphites. Materials Transactions, 2012, 53, 1159-1163.	1.2	16
149	The Novel Wetting Behavior of Periodic Ti <i>_x</i> Sn _{1−} <i>_x</i> O ₂ Nanostructures. Materials Transactions, 2012, 53, 191-194.	1.2	1
150	Effects of Alkali Corrosion Preprocessing on the Growth of Aligned Silver Nanorods Array and Its Improvement for Surface-Enhanced Raman Scattering. Materials Transactions, 2012, 53, 1278-1281.	1.2	0
151	Photocatalytic properties of TiO2 thin films obtained by glancing angle deposition. Applied Surface Science, 2012, 258, 2766-2770.	6.1	30
152	Enhanced room-temperature ferromagnetism in un-doped ZnO thin films by thermal annealing in a strong magnetic field. Journal of Applied Physics, 2012, 111, 103524.	2.5	16
153	Rapid Detection and Recognition of Organic Pollutants at Trace Levels by Surface-Enhanced Raman Scattering. , 2012, , .		ο
154	Enhanced surface-enhanced Raman scattering performance by folding silver nanorods. Applied Physics Letters, 2012, 100, .	3.3	54
155	Substrate effect on the room-temperature ferromagnetism in un-doped ZnO films. Applied Physics Letters, 2012, 101, .	3.3	36
156	Oxygen vacancy–induced ferromagnetism in un-doped ZnO thin films. Journal of Applied Physics, 2012, 111, .	2.5	125
157	Latticing vertically aligned Ag nanorods to enhance its SERS sensitivity. Materials Research Bulletin, 2012, 47, 921-924.	5.2	20
158	Surface-enhanced Raman scattering from helical silver nanorod arrays. Chemical Communications, 2011, 47, 4466.	4.1	46
159	Optical Properties and Surface Enhanced Raman Scattering of L-Shaped Silver Nanorod Arrays. Journal of Physical Chemistry C, 2011, 115, 14131-14140.	3.1	26
160	Preparation of Highly Textured ZnO Thin Films by Pulsed Electron Deposition. Materials Transactions, 2011, 52, 1764-1767.	1.2	4
161	A Simple Model to Describe the Rule of Glancing Angle Deposition. Materials Transactions, 2011, 52, 469-473.	1.2	46
162	Preparation and Photocatalytic Property of TiO ₂ Columnar Nanostructure Films. Materials Transactions, 2011, 52, 1939-1942.	1.2	15

#	Article	IF	CITATIONS
163	Surface-enhanced Raman scattering from a hexagonal lattice of micro-patterns of vertically aligned Ag nanorods. Physica E: Low-Dimensional Systems and Nanostructures, 2011, 44, 460-463.	2.7	19
164	Magnetic and Microwave Absorption Properties of Core/Shell FeCo-Based Nanocomposites Synthesized by a Simple Wet Chemical Method. IEEE Transactions on Magnetics, 2011, 47, 3456-3459.	2.1	6
165	Thermal stability and sputtering resistance under irradiation of yttria dispersed ferrum films. Rare Metals, 2011, 30, 258-261.	7.1	0
166	Influence of vacuum annealing and irradiation on magnetic properties of Fe-3%Y2O3 films. Rare Metals, 2011, 30, 453-457.	7.1	0
167	Anisotropic Ti x Sn1- x O2 nanostructures prepared by magnetron sputter deposition. Nanoscale Research Letters, 2011, 6, 326.	5.7	14
168	Openâ€Ended, Nâ€Doped Carbon Nanotube–Graphene Hybrid Nanostructures as Highâ€Performance Catalyst Support. Advanced Functional Materials, 2011, 21, 999-1006.	14.9	358
169	Fabrication and characterization of polycrystalline silicon nanowires with silver-assistance by electroless deposition. Applied Surface Science, 2011, 257, 3861-3866.	6.1	31
170	Oxygen deficient V2O5 nanorods for gas sensing. Physica E: Low-Dimensional Systems and Nanostructures, 2011, 43, 1726-1729.	2.7	10
171	Thermal Stability of HfO ₂ Nanostructures as Antireflection Coatings. Nanoscience and Nanotechnology Letters, 2011, 3, 731-734.	0.4	2
172	Growth of [010] oriented α-MoO ₃ nanorods by pulsed electron beam deposition. Applied Physics Letters, 2011, 99, 223104.	3.3	19
173	The synthesis and photoluminescence properties of selenium-treated porous silicon nanowire arrays. Nanotechnology, 2011, 22, 075203.	2.6	18
174	Contrastive Analysis of the Raman Spectra of Polychlorinated Benzene: Hexachlorobenzene and Benzene. Sensors, 2011, 11, 11510-11515.	3.8	29
175	Rapid Detection of Polychlorinated Biphenyls at Trace Levels in Real Environmental Samples by Surface-Enhanced Raman Scattering. Sensors, 2011, 11, 10851-10858.	3.8	16
176	Fabrication and Optical Property of Periodic <mml:math xmlns:mml="http://www.w3.org/1998/Math/MathML"><mml:msub><mml:mrow><mml:mtext>Sn</mml:mtext><!--<br-->Patterned by the Polystyrene Mic. Journal of Nanomaterials, 2011, 2011, 1-7.</mml:mrow></mml:msub></mml:math 	/mamil:mrov	₩7 < mml:mr
177	Irradiation Induced Localized Amorphization in Mo-Re Alloy Films. Materials Transactions, 2010, 51, 670-674.	1.2	2
178	Rapid recognition of isomers of monochlorobiphenyls at trace levels by surface-enhanced Raman scattering using Ag nanorods as a substrate. Nano Research, 2010, 3, 423-428.	10.4	59
179	Realignment of slanted Fe nanorods on silicon substrates by a strong magnetic field. Nano Research, 2010, 3, 438-443.	10.4	8
180	Rapid detection of 2, 3, 3′, 4, 4′-pentachlorinated biphenyls by silver nanorods-enhanced Raman spectroscopy. Physica E: Low-Dimensional Systems and Nanostructures, 2010, 42, 1717-1720.	2.7	34

#	Article	IF	CITATIONS
181	The effect of underlayer thin films on the surface-enhanced Raman scattering response of Ag nanorod substrates. Applied Physics Letters, 2010, 97, .	3.3	49
182	Effect of magnetic field on the visible light emission of V2O5 nanorods. Applied Physics Letters, 2009, 94, .	3.3	38
183	Novel Ag–Cu substrates for surface-enhanced Raman scattering. Materials Letters, 2009, 63, 2306-2308.	2.6	50
184	Fabrication of silver-coated silicon nanowire arrays for surface-enhanced Raman scattering by galvanic displacement processes. Applied Surface Science, 2009, 256, 916-920.	6.1	36
185	Nanostructuring HfO ₂ Thin Films as Antireflection Coatings. Journal of the American Ceramic Society, 2009, 92, 3077-3080.	3.8	25
186	Synthesis and field emission property of VO2 nanorods with a body-centered-cubic structure. Physica E: Low-Dimensional Systems and Nanostructures, 2009, 41, 548-551.	2.7	25
187	Ion-implantation-induced patterns formation on silicon substrates. Physica E: Low-Dimensional Systems and Nanostructures, 2009, 41, 833-837.	2.7	11
188	Facile Synthesis of α-Fe ₂ O ₃ Nanostructured Films with Controlled Morphology. Materials Transactions, 2009, 50, 1351-1354.	1.2	13
189	Photoluminescence of amorphous niobium oxide films synthesized by solid-state reaction. Thin Solid Films, 2008, 516, 4213-4216.	1.8	14
190	Arrays of aligned, single crystalline silver nanorods for trace amount detection. Journal Physics D: Applied Physics, 2008, 41, 152007.	2.8	81
191	Nanostructured VO ₂ Photocatalysts for Hydrogen Production. ACS Nano, 2008, 2, 1492-1496.	14.6	162
192	Rapid, low-temperature synthesis of single-crystalline Co ₃ O ₄ nanorods on silicon substrates on a large scale. Nanotechnology, 2008, 19, 155606.	2.6	97
193	Enhanced photocatalytic activity of porous α-Fe ₂ O ₃ films prepared by rapid thermal oxidation. Journal Physics D: Applied Physics, 2008, 41, 202002.	2.8	50
194	Oxygen defect induced photoluminescence of HfO2 thin films. Applied Physics Letters, 2008, 93, .	3.3	59
195	Synthesis and optical properties of V2O5 nanorods. Journal of Chemical Physics, 2007, 126, 164701.	3.0	61
196	Influence of deposition conditions on the morphology and phase of tungsten oxide nanorods synthesized by thermal oxidation. Frontiers of Materials Science in China, 2007, 1, 16-19.	0.5	1
197	Synthesis of silicon carbide nanowires by solid phase source chemical vapor deposition. Frontiers of Materials Science in China, 2007, 1, 304-308.	0.5	9
198	Growth control of tungsten oxide nanostructures on planar silicon substrates. Applied Physics Letters, 2006, 89, 193111.	3.3	25

#	Article	IF	CITATIONS
199	NiO films consisting of vertically aligned cone-shaped NiO rods. Applied Physics Letters, 2006, 88, 033101.	3.3	83
200	Intense photoluminescence from amorphous tantalum oxide films. Applied Physics Letters, 2006, 89, 021915.	3.3	72
201	Melting and optical properties of ZnO nanorods. Applied Physics Letters, 2006, 88, 061913.	3.3	81
202	Selecting the growth sites of carbon nanotubes on silicon substrates by ion implantation. Applied Physics Letters, 2006, 88, 263115.	3.3	5
203	Selective growth of graphite micro-rods with SiO2 nanowire cores by chemical vapor deposition. Applied Physics Letters, 2006, 88, 113102.	3.3	2
204	GROWTH CARBON NANOTUBES DIRECTLY ON PRISTINE SILICON SUBSTRATES. International Journal of Nanoscience, 2006, 05, 433-438.	0.7	1
205	From carbon nanotube crystals to carbon nanotube flowers. Tsinghua Science and Technology, 2005, 10, 741-744.	6.1	2
206	Tuning the Field-Emission Properties of Tungsten Oxide Nanorods. Small, 2005, 1, 310-313.	10.0	116
207	From zinc nanowires to zinc oxide nanowires: a low substrate-temperature approach. Journal Physics D: Applied Physics, 2005, 38, 1068-1071.	2.8	28
208	Control the relative length of carbon nanotubes from site to site on one silicon substrate. Applied Physics Letters, 2005, 87, 223121.	3.3	11
209	Synthesis and self-organization of γ-Fe2O3 nanoparticles by hydrothermal chemical vapor deposition. Materials Letters, 2005, 59, 3375-3377.	2.6	18
210	Synthesis and photoluminescence of aligned ZnO nanorods by thermal decomposition of zinc acetate at a substrate temperature of â^1⁄4250 °C. Journal Physics D: Applied Physics, 2005, 38, 3934-3937.	2.8	41
211	Characterization of Fe nanorods grown directly from submicron-sized iron grains by thermal evaporation. Physical Review B, 2004, 70, .	3.2	16
212	Optical and dielectric properties of a nanostructured NbO2 thin film prepared by thermal oxidation. Journal Physics D: Applied Physics, 2004, 37, 3392-3395.	2.8	82
213	Enhanced field emission properties of MoO2 nanorods with controllable shape and orientation. Materials Letters, 2004, 58, 3812-3815.	2.6	60
214	Preparation of MoO3nanostructures and their optical properties. Journal of Physics Condensed Matter, 2003, 15, L547-L552.	1.8	67
215	Low-temperature synthesis of large-scale arrays of aligned tungsten oxide nanorods. Journal of Physics Condensed Matter, 2003, 15, L453-L461.	1.8	65
216	Self-networking of carbon nanotubes. Chemical Communications, 2002, , 962-963.	4.1	9

#	Article	IF	CITATIONS
217	Self-assembled patterns of iron oxide nanoparticles by hydrothermal chemical-vapor deposition. Applied Physics Letters, 2001, 79, 4207-4209.	3.3	42
218	The Detection of Organic Pollutants at Trace Level by Variable Kinds of Silver Film with Novel Morphology. , 0, , .		0
219	Enhanced Visible Light Photocatalytic Performance by Nanostructured Semiconductors with Glancing Angle Deposition Method. , 0, , .		2
220	Electrochemical Materials Design for Micro-Supercapacitors. , 0, , .		2